

## ORIGINAL RESEARCH ARTICLE

# Numerical investigation on light non-aqueous phase liquid flow in the vadose zone considering porosity effects on soil hydraulic properties

Jia-ren Yu<sup>1</sup>  | Chao Zhou<sup>1</sup>  | Qing Yi Mu<sup>1,2</sup> 

<sup>1</sup>Dep. of Civil and Environmental Engineering, The Hong Kong Polytechnic Univ., Hung Hom, Hong Kong

<sup>2</sup>Dep. of Civil Engineering, Xi'an Jiaotong Univ., Xi'an, China

## Correspondence

Chao Zhou, Dep. of Civil and Environmental Engineering, The Hong Kong Polytechnic Univ., Hung Hom, Hong Kong.

Email: [c.zhou@polyu.edu.hk](mailto:c.zhou@polyu.edu.hk)

Assigned to Associate Editor Kevin Mumford.

## Funding information

National Natural Science Foundation of China, Grant/Award Number: 52022004; Research Grants Council, University Grants Committee, Grant/Award Number: 16204817; Technology Innovation Center for Land Engineering and Human Settlements, Grant/Award Number: 201912131-A1; Natural Science Foundation of Shaanxi Province, Grant/Award Number: 2020JQ-041

## Abstract

In the management of light non-aqueous phase liquid (LNAPL)-contaminated ground, numerical simulation is widely used to analyze LNAPL flow in the unsaturated soil (vadose) zone. Porosity effects on the hydraulic properties of unsaturated soils are highly simplified in existing mathematical models. Some important features, such as the nonlinear relation between porosity and permeability/displacement pressure, cannot be well captured. To address this problem, a new mathematical model was developed in this study, considering porosity effects on hydraulic properties of soils, including the retention behavior and permeability function of LNAPL and water. The newly developed model was implemented in MATLAB using the finite difference method and then verified by the results of a centrifuge test. Then, parametric studies were conducted to investigate the flow of LNAPL upon an active leakage at the ground surface. Based on the computed results, the influence of several factors, such as porosity magnitude, porosity distribution, and soil layering, was revealed. In particular, an increase in the porosity leads to a significant increase in the volume of LNAPL leaked into the ground, the vertical front depth, and the area of contaminated ground. This is mainly because the porosity affects not only the intrinsic permeability but also the relative permeability because (a) the intrinsic permeability of soils is larger at a higher porosity (b) when the porosity is higher, the equilibrium water saturation at a given capillary pressure is smaller. Consequently, LNAPL can achieve a larger degree of saturation and higher relative permeability.

## 1 | INTRODUCTION

Soil and groundwater contamination by light non-aqueous phase liquid (LNAPL) is a very common problem in industrial sites such as petrol stations, vehicle repair workshops, and oil

refineries. In the management of contaminated sites, it is a prerequisite to determine the influence zone and the distribution of LNAPL in the vadose zone (Lenhard et al., 2017, 2018; McWhorter & Sunada, 1990; Rivett et al., 2014; Sale et al., 2018; Schmid et al., 2011). In practice, discrete monitoring wells can be constructed to measure the LNAPL thickness and saturation (Aral & Liao, 2000; Jeong & Charbeneau, 2014). The in situ monitoring results are often analyzed together with

**Abbreviations:** LNAPL, light non-aqueous phase liquid; WRC, water retention curve.

This is an open access article under the terms of the [Creative Commons Attribution-NonCommercial-NoDerivs](https://creativecommons.org/licenses/by-nc-nd/4.0/) License, which permits use and distribution in any medium, provided the original work is properly cited, the use is non-commercial and no modifications or adaptations are made.

© 2022 The Authors. *Vadose Zone Journal* published by Wiley Periodicals LLC on behalf of Soil Science Society of America.

numerical simulations to provide a spatio-temporal distribution of LNAPL in detail (Jackson et al., 2006; Sharmin & Gabr, 2012). In addition, numerical analysis is also an important and efficient method for the optimization of LNAPL remediation and recovery (Sookhak Lari et al., 2019). Lari et al. (2018) recently conducted 80 numerical simulations of representative multi-phase flow scenarios and concluded that an appropriate numerical approach could accurately assess the effectiveness of LNAPL remedial and recovery methods under complex ground conditions. Hence, an accurate numerical prediction of LNAPL flow and distribution is very useful for engineering practices.

So far, many numerical models have been developed for simulating LNAPL flow, such as NAPL Simulator (Guarnaccia et al., 1997), STOMP (White & Oostrom, 2003), TMVOC (Pruess & Battistelli, 2002), and PFLOTRAN (Hammond et al., 2014). Their advantages and strengths were discussed in detail by Lari et al. (2019) in a comprehensive review. In each model, the hydraulic properties of unsaturated soils, including the retention behavior and the permeability function of water and LNAPL, play an essential role. The modeling of them is challenging, given the complicated LNAPL–air–water–soil interaction. Previous researchers have made great contributions to incorporating more factors and improving model capability. For instance, Falta et al. (1995) proposed and incorporated a tortuosity factor, which is the ratio of an average length of microscopic flow paths to the length of the macroscopic flux system. Pruess (2004) incorporated hydraulic hysteresis, which is the dependency of capillary effects on the drainage and imbibition history. Pasha et al. (2014) compared the computed results with and without hysteresis and concluded that the nonhysteretic model slightly underestimated the LNAPL flow in the vadose zone. The importance of hysteresis was also reported by other researchers, like Lari, Davis, et al. (2016). In addition, some research revealed that LNAPL partitioning (volatilization into gaseous phase and dissolution into aqueous phase) could alter fluid properties such as the surface tension and affect LNAPL flow, particularly in the long-term condition (Lari, Johnston, et al., 2016; Lekmine et al., 2017).

Although previous studies incorporated a number of factors in the numerical models, as illustrated above, porosity effects were highly simplified. Leverett and Lewis (1941) assumed a linear relationship between porosity and saturated permeability, but the permeability–porosity relation of soils is usually nonlinear (see detailed discussion in Section 2). Delshad et al. (2002) incorporated effective porosity, which is the ratio of the volume of the conducting pores to the total volume (Koponen et al., 1997), but the influence of effective porosity on hydraulic properties was not considered. More importantly, the retention behavior of water and LNAPL is generally described by the constitutive relationships of Brooks and Corey (1964) and van Genuchten (1980)

### Core Ideas

- A new theoretical model is developed, considering porosity effects on soil hydraulic properties.
- The model capability is verified using the results of a centrifuge test.
- The results of parametric studies have revealed the importance of porosity effects.

because these two models give good predictions of capillary pressure–saturation relation. The influence of porosity on the retention behavior is not incorporated, even though it has been revealed by extensive experimental investigations (Cui et al., 2003; Gallage & Uchimura, 2010; Salager et al., 2013). Cui et al. (2003) measured the LNAPL retention curves of a clay at different porosities (0.36, 0.41, and 0.52). They found that at a lower porosity, the LNAPL retention ability was higher because of smaller pore sizes. Salager et al. (2013) measured the water retention curves of a granular soil and a clayey soil. The results showed that a change in porosity could greatly affect the displacement pressure and the shape of water retention curve. To better predict the LNAPL flow, porosity effects on the hydraulic properties should be incorporated, considering that porosity in the field may vary spatially and temporally for different reasons, such as soil deformation under the action of self-weight and external loads. Note that porosity effects could be considered via the value of model parameters. When the porosity of specific soil changes, it is modeled as another material with different parameter values. This method has some obvious drawbacks. From a theoretical perspective, it is more reasonable to model soil behavior at different porosities in a unified approach (Ng et al., 2020; A. Zhou et al., 2012; C. Zhou, Tai, et al., 2020). A unified approach requires more parameters, but it is able to model the behavior of a soil using a single set of parameters, irrespectively of its state, such as porosity and water/LNAPL content. From a practical perspective, a unified model can be readily used for coupled hydro-mechanical analysis, if necessary, where porosity may change during the water and LNAPL flow.

By using the existing numerical models, extensive studies have been conducted to investigate the influence of soil hydraulic properties on LNAPL flow. For instance, Lenhard and Parker (1990) found the influence of water/LNAPL retention behavior on LNAPL flow upon the leakage of LNAPL. Beckett and Huntley (1998) simulated the LNAPL remediation in coarse-grained and fine-grained soils. They found a higher remediation efficiency in the coarse-grained soil due to its higher intrinsic permeability. A similar finding was reported by Lari et al. (2018). Soga et al. (2003) and Yang et al. (2013) conducted centrifuge tests and numerical

simulations on LNAPL flow in unsaturated layered soils. The results indicated that LNAPL infiltration and entrapment in layered soils were affected by the subsurface soil structures, initial water saturation, and LNAPL infiltration rate. In addition, some researchers studied the effect of soil heterogeneity. Johnston and Trefry (2009) used the Monte Carlo approach and heterogeneous models with correlated vertical permeability distributions. The results indicate that the heterogeneous models are better for layering soils. Yoon et al. (2008) evaluated the effects of permeability heterogeneity and concluded that heterogeneous ground would cause more trapped LNAPL during remediation. The variables used in these heterogeneity studies concentrate on permeability, and the relationship between porosity and permeability is not considered.

Based on the above literature review, to fully understand the flow and distribution of LNAPL in various ground conditions, numerical studies should be carried out with consideration of porosity effects on soil hydraulic properties. In this study, a new model was therefore developed to simulate LNAPL flow. Different from existing models in the literature, the newly developed model considers porosity effects on the water/LNAPL retention behavior and water/LNAPL permeability function. Then, this model was implemented in MATLAB using the finite difference method and verified using a centrifuge test reported by Pasha et al. (2014). Finally, the new numerical code was applied to investigate the influence of porosity, soil type, and soil layering condition on LNAPL flow.

## 2 | A NEW MODEL FOR THE COUPLED WATER AND LNAPL FLOW WITH EFFECTS OF SOIL POROSITY

### 2.1 | Model assumptions

Light non-aqueous phase liquid-contaminated unsaturated soil is a complicated system and comprises four phases, including solid particle (S), liquid water (W), LNAPL (N), and air (A), as shown in Figure 1. Solid particles form the soil skeleton, the pores of which are filled with one or multiple types of fluids (i.e., water, LNAPL, and air). The variables defined in Equations A1–A9 in the Appendix are used to model soil hydraulic properties, which play a crucial role in LNAPL flow. The hydraulic properties include not only the water retention function and water permeability function but also the LNAPL retention function and LNAPL permeability function. The modeling of them is introduced in this section.

As illustrated in the Introduction, the coupled water and LNAPL flows in the vadose zone are very complicated. This study does not intend to consider all physical processes and influencing factors. Therefore, the following assumptions are

adopted for simplicity: (a) diffusion and dispersion among different phases and LNAPL partitioning are neglected, (b) water and LNAPL are incompressible and capillary pressure-induced soil volume changes are not considered, (c) air pressure is constant and equal to zero with reference to the atmospheric pressure, (d) the biodegradation of LNAPL is negligible for the time period under investigation, (e) phase change between liquid water and vapor water is not considered, (f) hydraulic hysteresis in the water/LNAPL retention curve and permeability function is not considered, and (g) effective porosity and tortuosity are not incorporated.

### 2.2 | Governing equations for the water flow

The mass balance equation and Darcy's law for the water phase are described by Equations B1 and B2 in the Appendix. The effective permeability in Equation B2 is a measure of soil's liquid conductivity. It is a function of the intrinsic permeability and relative permeability (Leong & Rahardjo, 1997; Mualem, 1976):

$$k_w = K k_{rw} \quad (1)$$

where  $K$  is the intrinsic permeability ( $m^2$ ), and  $k_{rw}$  is the relative permeability, which is the ratio of the permeability at a given saturation to the permeability at the saturated condition. These two variables are discussed in detail below:

1. The intrinsic permeability in Equation 1 is strongly dependent on soil type. Its typical range for various soils are as follows:  $10^{-14}$ – $10^{-19}$   $m^2$  (clay),  $10^{-12}$ – $10^{-15}$   $m^2$  (silt), and  $10^{-7}$ – $10^{-13}$   $m^2$  (sand) (Bear, 1988). Porosity is another important factor that affects intrinsic permeability. With consideration of these two effects, this study adopts the equation of Stoltz et al. (2010):

$$K = C_1(n)^{C_2} \quad (2)$$

where  $C_1$  ( $m^2$ ) and  $C_2$  are model parameters. Parameter  $C_1$  mainly describes the influence of soil type, and parameter  $C_2$  governs the sensitivity of permeability to porosity. When  $C_2$  is equal to 1, the equation is similar to the formulation of Leverett (1941) and predicts a linear relationship between permeability and porosity. At other  $C_2$  values, this equation predicts a nonlinear permeability–porosity relation. In Equation 2, the widely used formulations by Leverett (1941) and Carman (1939) are used to fit the experimental results of Zhang et al. (2020). The results are shown in Figure 2. It is clear that the relationship between permeability and porosity is nonlinear, and Equation 2 shows a better performance.

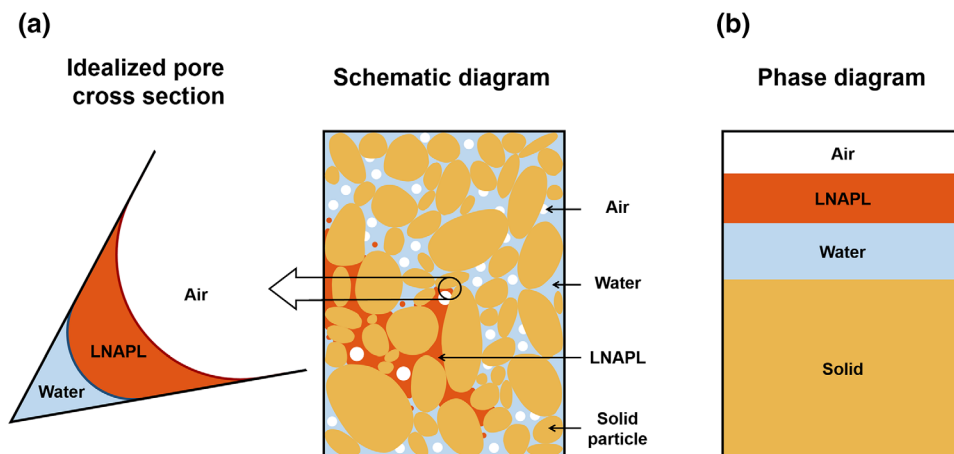


FIGURE 1 (a) Schematic diagram of light non-aqueous phase liquid (LNAPL)-contaminated unsaturated soil; (b) phase diagram

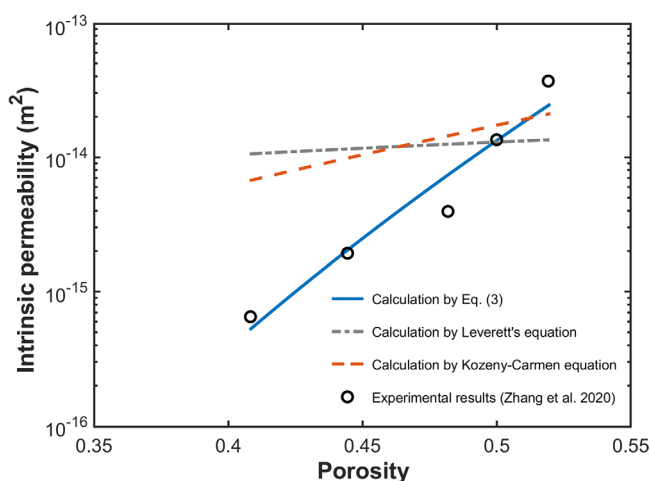


FIGURE 2 Porosity-intrinsic permeability relation of a clay: experimental data of Zhang et al. (2020) and fitted results using different equations

2. The relative permeability in Equation 1 is a scaling factor for considering saturation effects on permeability. Mualem (1976) proposed a method in which the pore size distribution is derived from the water retention curve (WRC) and then used to predict the relative permeability. By using this method, the relationship between relative permeability and water saturation (i.e., K–S relation) was derived by Parker et al. (1987) from the WRC model of van Genuchten (1980):

$$k_{rW} = \bar{S}_W \left[ 1 - \left( 1 - \bar{S}_W^{1/m} \right)^m \right]^2 \quad (3)$$

where  $\bar{S}_W$  is the effective water saturation, and  $m$  is a soil parameter in the van Genuchten model. This equation works for both LNAPL-free (three-phase) and LNAPL-contaminated (four-phase) soils (Parker et al., 1987).

Apart from water permeability, the application of Equation B1 requires another important input. It is the relationship between water saturation and capillary pressure (i.e., S–P relation). The WRC model of van Genuchten (1980) was modified and used by previous researchers (Parker et al., 1987) for this purpose:

$$P_{cNW} = \left[ (\bar{S}_W)^{-1/m} - 1 \right]^{1-m} \alpha^{-1} \beta_{NW}^{-1} \quad (4)$$

where  $P_{cNW}$  is the LNAPL–water capillary pressure;  $\alpha$  is a model parameter; and  $\beta_{NW}$  is a fluid type-dependent scaling factor, defined as the ratio of air–water interfacial tension to LNAPL–water interfacial tension. A detailed derivation of this equation is given in Appendix C. It has been verified by some experimental results (Busby et al., 1995), but it has an obvious limitation (i.e., without consideration of porosity effects). This limitation results in some problems from both theoretical and practical perspectives, as illustrated in the Introduction. During the past two decades, many researchers have investigated the influence of porosity on WRC (Ng & Pang, 2000; Tarantino, 2009; Zhang et al., 2020; C. Zhou & Chen, 2021; C. Zhou & Ng, 2014; C. Zhou, So, et al., 2020). For instance, Zhang et al. (2020) measured the WRCs of clay at various porosities. When the porosity was lower, the measured water retention ability was much higher. Some theoretical modellers (Gallipoli et al., 2003; Hu et al., 2013; Tarantino, 2009) summarized the data in the literature and found that, with a decrease in porosity, the displacement pressure becomes larger associated with a smaller  $\alpha$ , and the value of  $m$  can be approximated by a constant value. Based on these findings and the theoretical model of Tarantino (2009), the current study adopts the following equation to describe porosity effects on  $\alpha$ :

$$\alpha = a \left( \frac{n}{1-n} \right)^{(1/m-1)} \quad (5)$$



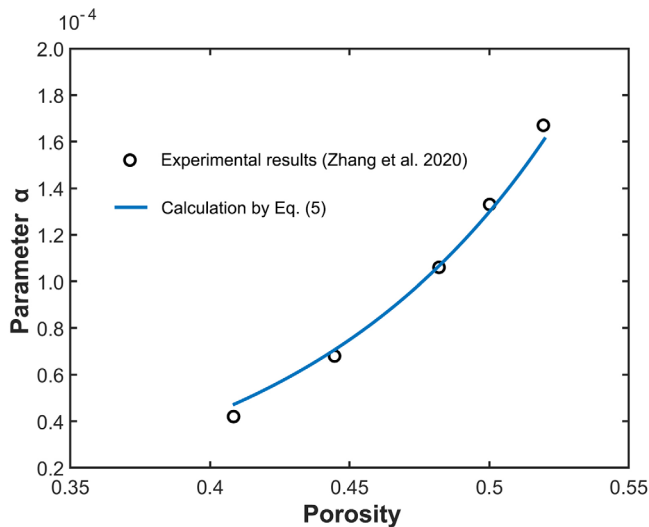


**FIGURE 3** The value of parameter  $\alpha$  versus porosity: experimental data of a clay (Zhang et al., 2020) and fitting results using Equation 5

where  $m$  is the parameter in the van Genuchten model (see Equation 4), and  $a$  is a new parameter associated with soil type. Equation 5 suggests that as soil porosity decreases,  $\alpha$  decreases, and hence displacement pressure and water retention ability increase. This equation is applied to fit the data of Zhang et al. (2020), and the results are shown in Figure 3. The effects of porosity on  $\alpha$  are clear and are well captured by the equation.

Substituting Equation 5 into Equation 4 yields

$$P_{cNW} = \left[ (\bar{S}_W)^{-1/m} - 1 \right]^{1-m} a^{-1} \left( \frac{n}{1-n} \right)^{(1-1/m)} \beta_{NW}^{-1} \quad (6)$$

This is the newly proposed equation for the WRC of LNAPL-contaminated unsaturated soils. Compared with existing equations in the literature, the porosity effects are incorporated by introducing the nonlinear  $\alpha$ - $n$  relation (i.e., Equation 5).

### 2.3 | Governing equations for the LNAPL flow

The mass conservation and Darcy's law for the LNAPL flow are described by Equations B3 and B4 in the Appendix. The application of them requires the effective permeability and retention function of LNAPL. The effective permeability is modeled using the following equation:

$$k_N = K k_{rN} \quad (7)$$

where  $K$  and  $k_{rN}$  are the intrinsic permeability and relative permeability of LNAPL, respectively. The intrinsic permeability

is calculated using Equation 2. The relative permeability is estimated from the retention curve using the method of Mualem (1976), as discussed above. To calculate the relative permeability, the LNAPL retention behavior should be modeled first. Leverett (1941) proposed an LNAPL retention model in which the total liquid saturation is a function of the air-LNAPL capillary pressure. Based on this model and Equation C2, the following equations can be derived (Parker et al., 1987):

$$P_{cAN} = \left[ (\bar{S}_t)^{-1/m} - 1 \right]^{1-m} \alpha^{-1} \beta_{AN}^{-1} \quad (8)$$

where  $P_{cAN}$  is the air-LNAPL capillary pressure,  $\bar{S}_t$  is the effective total liquid saturation,  $m$  and  $\alpha$  are the same soil parameters as those in Equation 4, and  $\beta_{AN}$  is the scaling factor defined as the ratio of air-water and air-LNAPL interfacial tension. These equations were verified by Busby et al. (1995). Substituting the  $\alpha$ - $n$  relation (i.e., Equation 5 into Equation 8) reveals that

$$P_{cAN} = \left[ (\bar{S}_t)^{-1/m} - 1 \right]^{1-m} a^{-1} \left( \frac{n}{1-n} \right)^{(1-1/m)} \beta_{AN}^{-1} \quad (9)$$

Using this newly derived equation, the LNAPL retention behavior can be predicted. Figure 4a shows the LNAPL behavior of a soil at two different porosities. It is clear that the LNAPL saturation is affected by two capillary pressures (i.e.,  $P_{cAN}$  and  $P_{cNW}$ ). In addition, porosity effects on the LNAPL retention behavior are very obvious.

By applying the method of Mualem (1976) and Equation 9, the relative permeability of LNAPL is derived:

$$k_{rN} = (\bar{S}_t - \bar{S}_W)^{1/2} \left[ \left( 1 - \bar{S}_W^{1/m} \right)^m - \left( 1 - \bar{S}_t^{1/m} \right)^m \right]^2 \quad (10)$$

Figure 4b shows the relative permeability of LNAPL. As expected,  $k_{rN}$  is affected by both LNAPL saturation and water saturation. At a condition of constant water content,  $k_{rN}$  shows a substantial increase as LNAPL increases. At a condition of constant LNAPL saturation, an increase in water saturation will cause a reduction in  $k_{rN}$  because the presence of water would reduce the connectivity of LNAPL.

### 3 | NUMERICAL IMPLEMENTATION AND CALIBRATION OF MODEL PARAMETERS

The mathematic equations are implemented in MATLAB based on the finite difference method. For spatial discretization, this study adopted the simple orthogonal grid system. Regarding temporal discretisation, the explicit method was

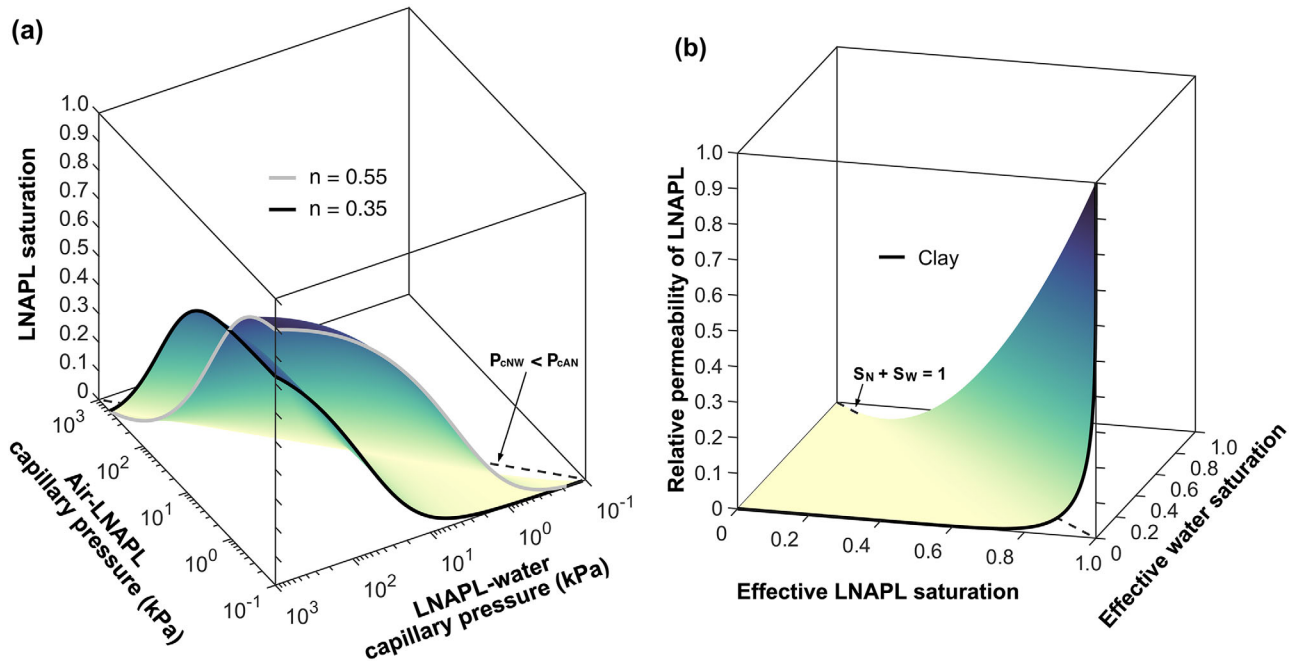


FIGURE 4 (a) Light non-aqueous phase liquid (LNAPL) retention curves with porosity effects and (b) relative permeability of LNAPL for clay

used. After the spatial and temporal discretisation, nonlinear algebraic equations were obtained and solved. To minimize numerical errors, a very small time increment was used for each step. In addition, a range of spatial and temporal discretization was tested to verify that the temporal and spatial steps are able to give stable results. Numerical analysis of coupled LNAPL and water flow is challenging because the governing equations are highly nonlinear and the ground conditions could be heterogeneous. Thus, many advanced numerical algorithms have been developed and discussed by previous researchers (e.g., Helmig & Huber, 1998; Parker et al., 1987). The principal objective of this study is to explore the influence of soil porosity by using a newly developed mathematical model. The scale of numerical analysis is relatively small, and the ground condition is simple. The computation efficiency was not a major concern, so the above simple numerical algorithm was used. If the new mathematical model is applied to carry out large-scale analysis with the complicated ground condition in the future, more advanced algorithms should be adopted.

Figure 5 shows the flow chart. The parameters for soil and liquid properties are input. The boundary condition (controlling the source-sink terms in Equations B1 and B3) and the initial condition (the distribution of capillary pressures and liquid saturations) are applied. After that, a computational cycle is finished for each time step using the explicit time integration scheme:

$$t^{(k+1)} = t^{(k)} + \Delta t \quad (11)$$

where  $k$  is the number of time steps, and  $\Delta t$  is the time increment. There are seven procedures in each time step:

- Calculate the air-LNAPL and LNAPL-water capillary pressures from the water saturation and LNAPL saturation using Equations 6 and 9
- Calculate the water pressure and LNAPL pressure from the two capillary pressures calculated in Step a:

$$P_N^{(k+1)} = P_A^{(k+1)} - P_{cAN}^{k+1} = -P_{cAN}^{(k+1)} \quad (12)$$

$$P_W^{(k+1)} = P_N^{(k+1)} - P_{cNW}^{k+1} \quad (13)$$

- Calculate the Darcy fluxes of water and LNAPL from the distribution of water and LNAPL pressures using Equations B2 and B4
- Update the water saturation and LNAPL saturation by using the calculated Darcy fluxes of water and LNAPL:

$$S_{eW}^{(k+1)} = S_{eW}^{(k)} - S_{eW}^{(k)} \Delta t \nabla \cdot \mathbf{v}_W \quad (14)$$

$$S_{eN}^{(k+1)} = S_{eN}^{(k)} - S_{eN}^{(k)} \Delta t \nabla \cdot \mathbf{v}_N \quad (15)$$

- Check the groundwater table level
- Update the relative permeabilities of water and LNAPL from the calculated saturations using Equations 3 and 10
- Finish the time step and go to the next one

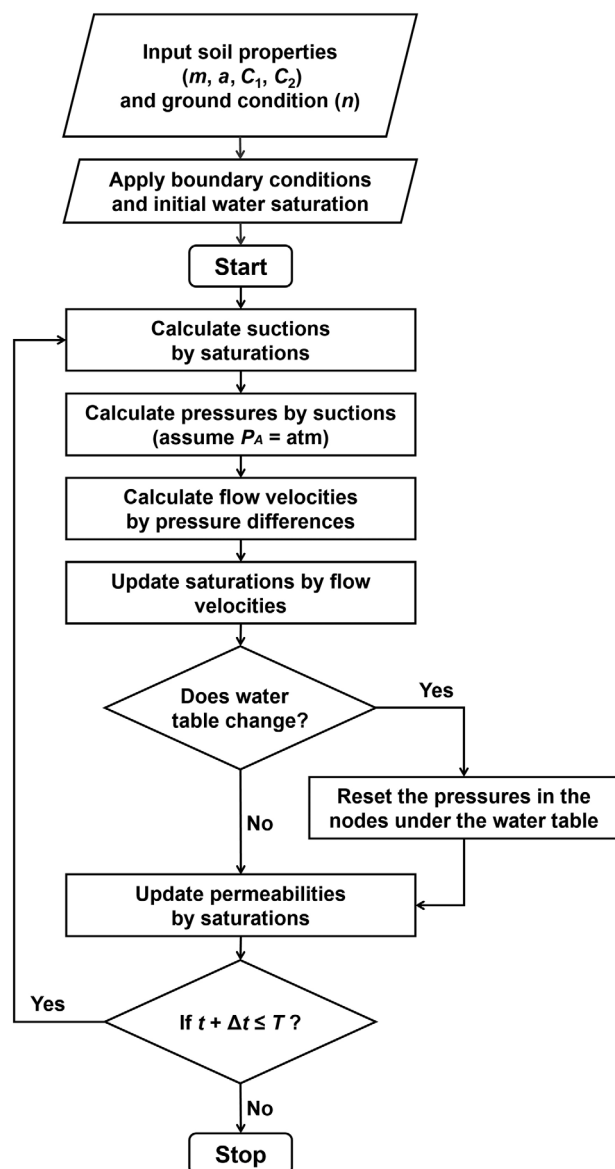


FIGURE 5 Flow chart of the new numerical model

This new numerical model is able to simulate various conditions. Four examples and the corresponding liquid pressures are summarized here: (a) water-saturated soil ( $P_W = P_N = P_A$ ), (b) LNAPL-saturated soil ( $P_W < P_N = P_A$ ), (c) LNAPL-free unsaturated soil ( $P_W < P_N = P_A$ ), and (d) LNAPL-contaminated unsaturated soil ( $P_W < P_N < P_A$ ).

There are 10 independent model parameters. Parameters  $\rho_W$ ,  $\rho_N$ ,  $\mu_W$ ,  $\mu_N$ ,  $T_{NW}$ , and  $T_{AN}$  are fluid parameters and can be determined readily based on the types of fluid. Parameters  $m$ ,  $a$ ,  $C_1$ , and  $C_2$  are soil parameters, and all of them can be calibrated from experimental results. The first three soil parameters are obtained by fitting the water retention curves at various densities, whereas the other two soil parameters are

determined from the relationship between water permeability and porosity.

## 4 | MODEL VERIFICATION USING A CENTRIFUGE TEST

The model performance was evaluated using the results of a centrifuge test reported by Pasha et al. (2014). The centrifugal test at the 50-g level was designed to study the two-dimensional flow of LNAPL in a fine-grained soil. In the prototype scale, LNAPL leaked for 27.2 d, and the test ended at 33.2 d. Details of this test were reported by Pasha et al. (2014). The numerical simulation in this study used the same soil and fluid parameters and the initial boundary conditions as the centrifugal test. In both the centrifuge test and the numerical simulation, the initial water saturation of compacted soil was 27%, and slight water redistribution occurred during the process of raising  $g$  level. After 10 d in the prototype scale, the water content along the depth reached an equilibrium condition. The water saturations are 20.9 and 31.2% at the ground surface and bottom boundary, respectively.

Figure 6a shows the contours of LNAPL saturation, deduced from the centrifuge test, at 27.2 d from the beginning of LNAPL leakage. Figure 6b shows the corresponding results of numerical simulation for comparison. The measured and computed results show good agreement on the distribution of LNAPL saturation. The wetting fronts of LNAPL at different times are summarized in Figure 6c (centrifugal test) and Figure 6d (numerical simulation). By comparing the measured and computed wetting front depths at different stages (Figures 6c,d), the average error is 5.9%. The measured and computed volumes of LNAPL leaked into the ground are shown in Figure 7. Despite some small differences (about 7% on average), the computed results agree well with the measured results. Figure 8 shows the profile of LNAPL saturation at the center line of the plume after 27.2-d leakage. The differences between measured and computed results are generally <10%.

Pasha et al. (2014) simulated the same centrifuge test by using the NAPL simulator (Guarnaccia et al., 1997). Their results are also included in Figures 7 and 8 for comparison. It can be seen that the results computed using the two models are comparable. Both models are able to well predict LNAPL flow in the unsaturated ground. The two models give very close results because the porosity distribution in the centrifuge test is uniform. If a nonuniform porosity distribution is encountered, the predictions would be more different because only the new model is able to capture porosity effects on soil hydraulic properties. After this verification, the new model is applied to carry out parametric studies, as shown in the following section.

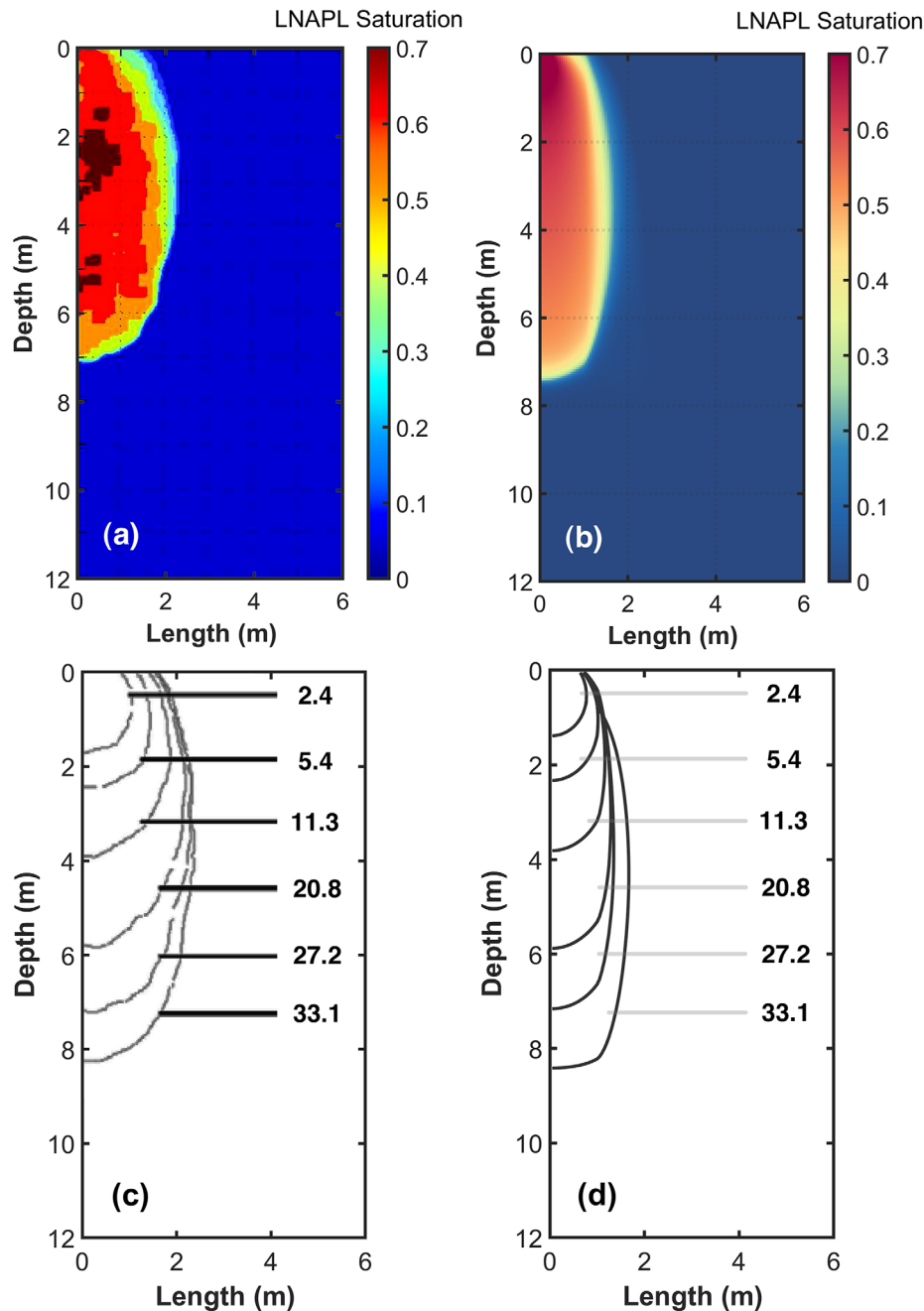


**FIGURE 6** Model verification using the results of a centrifuge test: (a) measured light non-aqueous phase liquid (LNAPL) saturation contours; (b) computed LNAPL saturation contour in Series A; (c) measured LNAPL wetting fronts (numbers are the days after start of LNAPL leak); (d) measured LNAPL wetting fronts

## 5 | NUMERICAL SIMULATION PROGRAM AND PROCEDURES OF THE PARAMETRIC STUDIES

Four series of parametric studies were carried out to investigate the influence of soil porosity, soil type, and soil layering condition on LNAPL flow, as summarized in Table 1. These parameters were selected for two reasons: (a) they are expected to greatly affect the hydraulic properties and LNAPL

flow and (b) a site investigation is one of the foremost steps for evaluating contamination and planning remediation. Soil porosity, soil type, and layering condition can be readily determined in the field. A study of these parameters can improve our understanding of LNAPL flow in various ground conditions. The value of each parameter is determined based on experimental data in the literature, as shown in Table 1.

Series B1 is designed to investigate the influence of porosity on LNAPL flow in clay. The porosity varies from 0.408 to



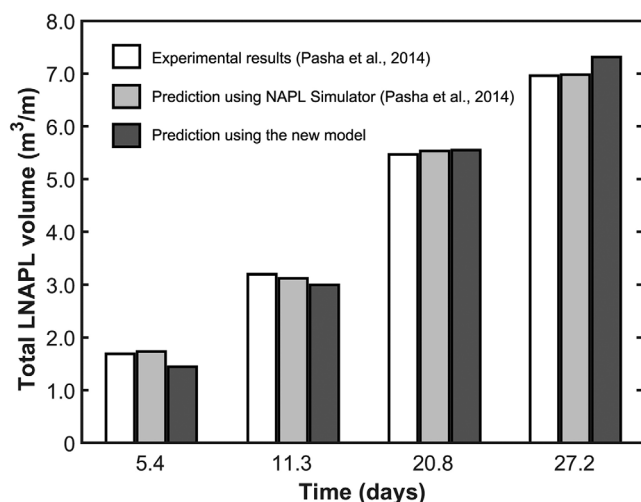


**FIGURE 7** Model verification using the results of a centrifuge test (Pasha et al., 2014): total light non-aqueous phase liquid (LNAPL) volume in the ground

0.519 (corresponding to five dry densities: 1.60, 1.50, 1.40, 1.35, and 1.30 g cm<sup>-3</sup>), and it is uniform along with the depth in each model. In Series B2 (the same clay as Series B1), descent porosity with depth is applied, considering that such a porosity distribution is very common in the field. By comparing with the results from Series B1, the influence of porosity distribution on LNAPL flow can be revealed. For the case of descent porosity distribution,  $n$  is estimated from the compression curve and the distribution of overburden pressure. To investigate the influence of soil type, three different soils are adopted in Series B3. To eliminate the effect of descent porosity, the porosities in Series B3 are uniform. The porosities of silt and sand are 0.51 and 0.34, respectively. In Series B4, the influence of layering is investigated. There are two combinations of soil layering: silt-clay is silt in the top 2 m and clay in the bottom 10 m. In all series of numerical simulations, the water table is at a depth of 12 m. Prior to LNAPL infiltration, water pressure follows the hydrostatic distribution. The corresponding water content distribution is calculated by the code and is dependent on the water retention behavior of soils. Table 2 shows the properties of sand, silt, and clay adopted in the above parametric studies. The clay considered in this study is of low plasticity. Its water retention curves at various porosities were measured by Zhang et al. (2020). The measured displacement pressures fall in the range of 5–25 kPa, depending on the value of porosity, meaning that the height of capillary rise is about 0.5–2.5 m, much smaller than the thickness of the soil layer above the water table.

Figure 9 shows the numerical domain for the parametric studies. The sizes of the nodes (215 × 110) vary from 0.05 to 0.2 m. In each simulation from Series B1–B4, the initial water distribution was theoretically calculated to reach a steady state condition. The distribution of air–water capillary pressure and water saturation is mainly affected by the retention behavior

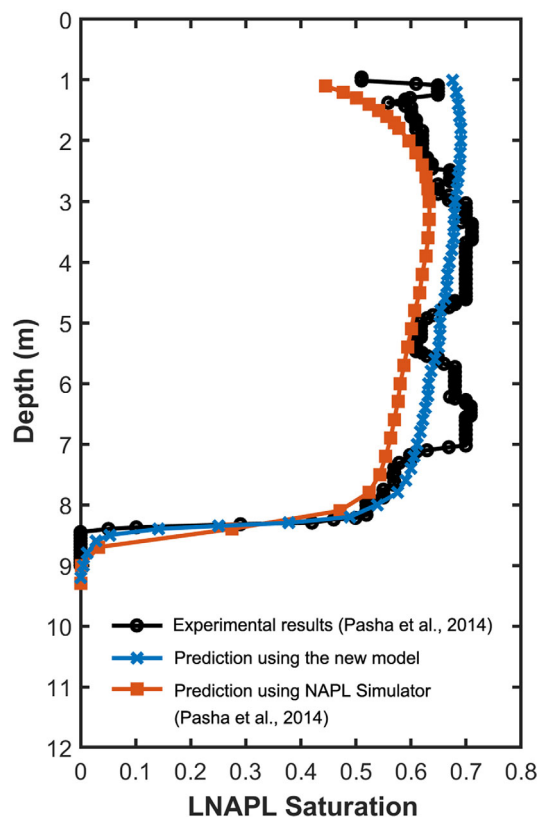


**FIGURE 8** Model verification using the results of a centrifuge test (Pasha et al., 2014): light non-aqueous phase liquid (LNAPL) saturation profiles at the center line of the plume after 27.2 d

of soils. After that, LNAPL was simulated with the following boundary conditions. (a) Boundary Condition a (denoted using inverted red triangles) is applied at the left side of the ground surface and represents the LNAPL leakage zone, in which the LNAPL pressure head was maintained at 0.3 m during the leakage period and the air and water fluxes were zero. (b) Boundary Condition b (denoted using hollow triangles) was applied on the right side of the ground surface. It imposes zero flux for water and NAPL and zero pressure for air. (c) Along the left and right boundaries, Boundary Condition c (denoted using hollow cycles) was applied. It is zero flux for all air, water, and LNAPL. In addition, the groundwater table is maintained at the bottom Boundary Condition d (denoted by solid triangles), where zero water pressure was applied and the flux for air and LNAPL was zero.

## 6 | RESULTS OF PARAMETRIC STUDIES AND DISCUSSION

### 6.1 | Influence of porosity on LNAPL flow in the uniform clay ground

Figure 10 shows the distribution of LNAPL in the uniform clay ground at 36 mo, computed from Series B1. Five porosi-

**TABLE 1** Numerical simulation program for model verification and parametric studies

Series	Objective	ID and the corresponding ground condition
A	To verify the numerical model	V1: same soil properties and ground condition as the centrifugal test (Pasha et al., 2014)
B1	To investigate the influence of porosity (uniform)	UP1: $n = 0.408$ UP2: $n = 0.444$ UP3: $n = 0.482$ UP4: $n = 0.500$ UP5: $n = 0.519$ (Zhang et al., 2020)
B2	To investigate the influence of porosity distribution	DP1: $n$ decreases with depth from 0.482 DP2: $n$ decreases with depth from 0.519
B3	To investigate the influence of soil type	S1: uniform sand (Oostrom & Lenhard, 1998) S2: uniform silt (Jarvis & Messing, 1995) S3: uniform clay (same as UP2)
B4	To investigate the influence of soil layering	L1: silt–clay (top 2 m: silt; bottom 10 m: clay) L2: clay–silt (top 2 m: clay; bottom 10 m: silt)

Note. The properties and porosity of each soil are determined based on the experimental results reported in the given references.

**TABLE 2** Hydraulic properties of sand, silt, and clay

Parameters	Value		
	Clay (Zhang et al., 2020)	Silt (Jarvis & Messing, 1995)	Sand (Oostrom & Lenhard, 1998)
$m$	0.268	0.301	0.662
$a$	$1.3 \times 10^{-4}$	$7.2 \times 10^{-4}$	$8.2 \times 10^{-4}$
$C_1$	$8.30 \times 10^{-10}$	–	–
$C_2$	15.93	–	–

Note. Jarvis and Messing (1995) did not report the permeabilities of silt at different porosities, so a constant value of  $1.60 \times 10^{-14} \text{ m}^2$  is used for the silt's  $K$ , and therefore the values of  $C_1$  and  $C_2$  are not required. Similarly, a constant value of  $7.21 \times 10^{-11} \text{ m}^2$  is used for the sand.

ties ranging from 0.408 to 0.519 are considered. It is clear that the wetting front of LNAPL is greatly affected by porosity. Its vertical distance to the leakage source increases from 0.25 to 4.65 m as the porosity increases from 0.408 to 0.519. This is attributed to at least two different effects imposed by the porosity upon the hydraulic properties of soils: (a) the intrinsic permeability is much larger at a higher porosity and (b) a larger porosity results in a lower water retention capacity and hence a smaller initial water saturation (i.e., the condition prior to the leakage of LNAPL). The initial water saturation at the ground surface decreased from 53.9 to 33.3% as the porosity increased from 0.408 to 0.519. A smaller water saturation led to a higher LNAPL saturation and then to a larger relative permeability for LNAPL (see Equation 10).

Figure 11 shows the total volume of LNAPL leaked into the ground. Porosity effects on it may be divided into two stages at a time of about 3 mo for the conditions under investigation. At the first stage, the differences induced by a change in soil porosity are negligible. This is mainly because the LNAPL saturation is very low at this stage. The relative permeability of LNAPL is close to zero (see Figure 4b) and plays a dominant role in LNAPL flow. Because the relative permeability is assumed to be independent of porosity, the computed

LNAPL volumes at various porosities are very similar. At the second stage, the LNAPL saturation and its relative permeability become much larger. Consequently, the intrinsic permeability of soils dominates the predicted results and porosity effects become more obvious with an increase in time. Taking the LNAPL volume accumulated within 36 mo as an example, the largest value (i.e.,  $3.84 \text{ m}^3 \text{ m}^{-1}$  with  $n = 0.519$ ) is about 43 times the lowest one (i.e.,  $0.09 \text{ m}^3 \text{ m}^{-1}$  with  $n = 0.408$ ) because of a larger intrinsic permeability at a higher porosity. In addition, the existence of two stages is more obvious in the higher-porosity cases ( $n = 0.519$  and 0.500) because soils with a higher porosity have a lower initial water saturation, as explained above. The saturation and relative permeability of LNAPL can therefore have a larger increment.

To further investigate the influence of porosity, the values of four variables (i.e., the vertical front depth, the horizontal front distance, the total LNAPL volume, and the area of contaminated ground) at 36 mo are shown in Figure 12. Each variable increases nonlinearly with an increase in porosity, at an increasing rate. When the porosity is below 0.45, the variation of porosity does not have a significant effect. If the porosity exceeds 0.45, however, porosity effects increase

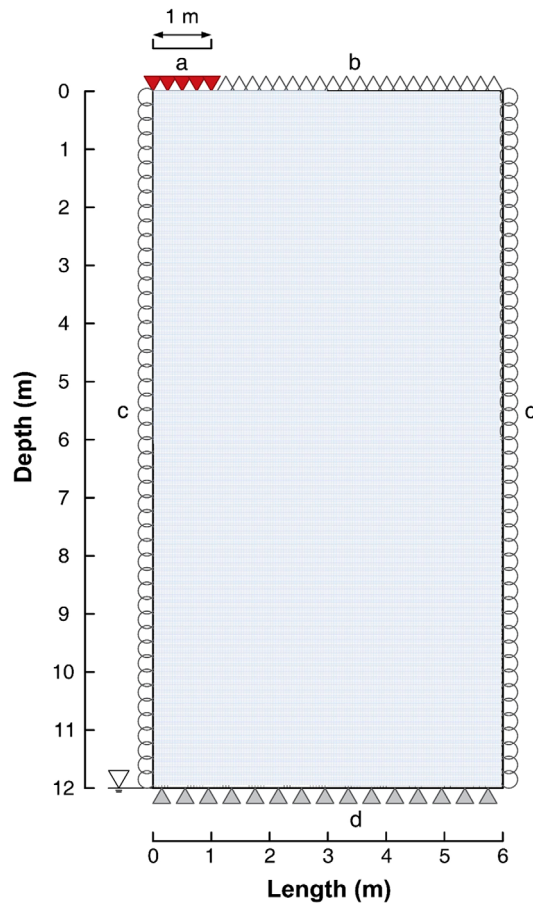


**FIGURE 9** The numerical domain and the boundary conditions. (a) The light non-aqueous phase liquid (LNAPL) leakage zone where the pressure head of LNAPL is 0.3 m; (b) zero flux for water and LNAPL; (c) impermeable for water and LNAPL; (d) water table where the water pressure is zero and the LNAPL flux is zero

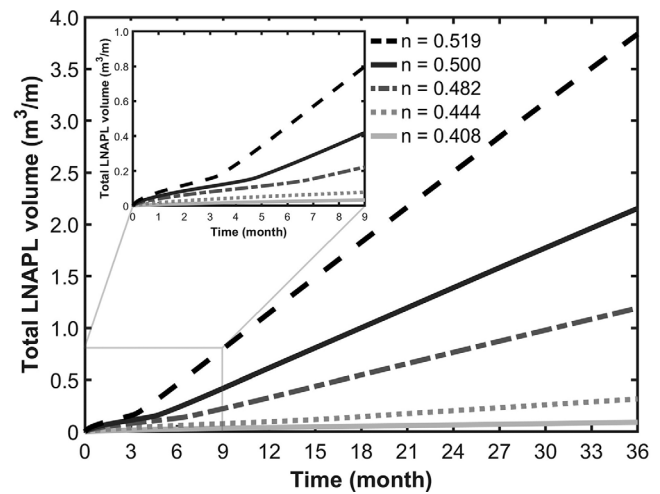


**FIGURE 11** Influence of porosity (uniform) through Series B1: total light non-aqueous phase liquid (LNAPL) volume

substantially. The observed nonlinearity is mainly due to the power function (i.e., Equation 2) relationship between porosity and the intrinsic permeability of soils.

Based on the above analysis, it can be concluded that LNAPL flow is highly related to soil porosity, particularly in the long term. This finding may help practical engineers to predict or minimize LNAPL flow. For example, in the design of petrol and gas stations as well as industrial sites, heavy compaction is desired to control potential LNAPL contamination. Furthermore, soil type is generally considered in the studies on the flow and distribution of LNAPL (Beckett & Huntley, 1998; Lari et al., 2018; Oostrom & Lenhard, 1998). This is not sufficient because the porosity of a given soil can vary widely, depending on the geological history and loading path. To improve the accuracy of numerical

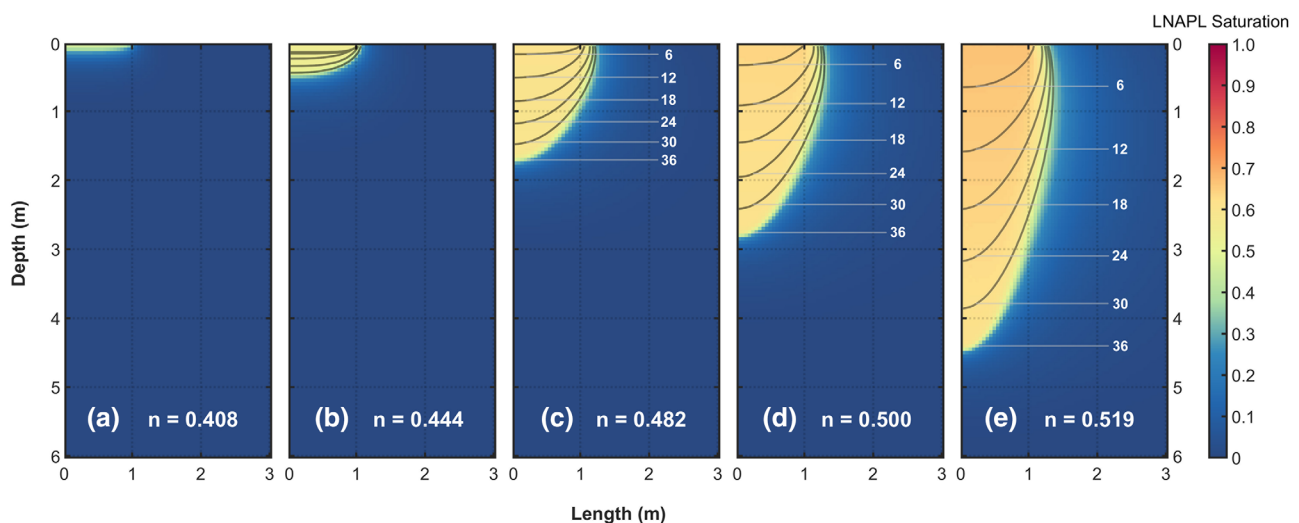


**FIGURE 10** Influence of porosity (uniform) through Series B1: light non-aqueous phase liquid (LNAPL) distribution contours at 36 mo and LNAPL fronts (numbers are the months after start of LNAPL leak)

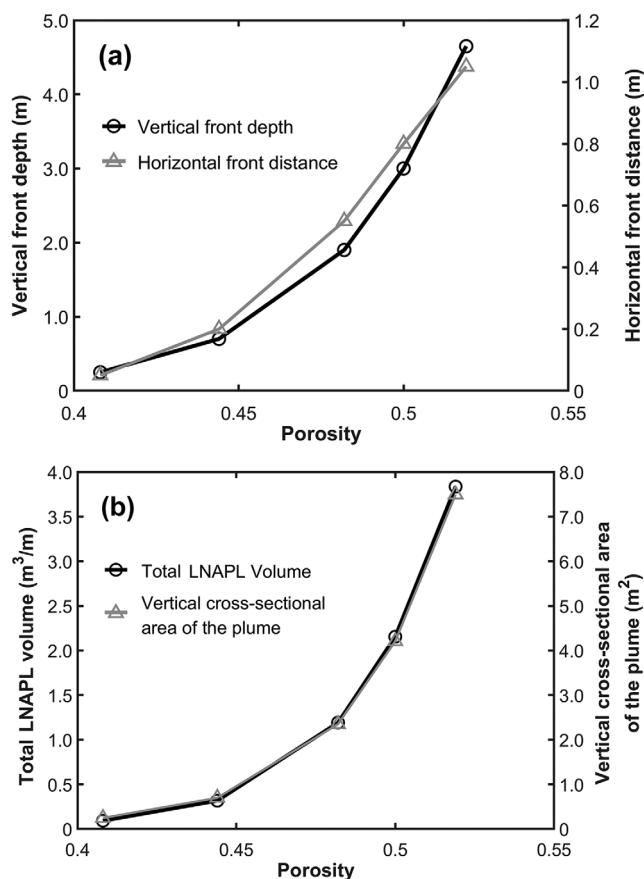


**FIGURE 12** Influence of porosity (uniform) through Series B1: (a) vertical front depth and horizontal front distance; (b) total light non-aqueous phase liquid (LNAPL) volume and vertical cross-sectional area of the plume

simulations, a porosity close to the in situ condition should be used.

## 6.2 | Influence of porosity distribution on LNAPL flow in the heterogeneous clay ground

Figure 13 shows the influence of porosity on the total LNAPL volume leaked into the clay ground. Two cases are compared in Series B2, including uniform porosity and descent porosity along with the depth. For each case, two different porosities at the ground surface ( $n = 0.482$  and  $0.519$ ) are used. When the porosity distribution is changed from uniform to descent condition, the accumulation rate of LNAPL volume keeps approximately constant at the early stage but then significantly reduces. Furthermore, this trend is more significant when the surface porosity is higher (i.e.,  $n = 0.519$ ). Compared with the case of descent porosity, the total LNAPL volume at 36 mo in the case of uniform porosity is about 3.5 and 2.5 times larger when the surface porosity is 0.519 and 0.482, respectively. This can be explained using the results in

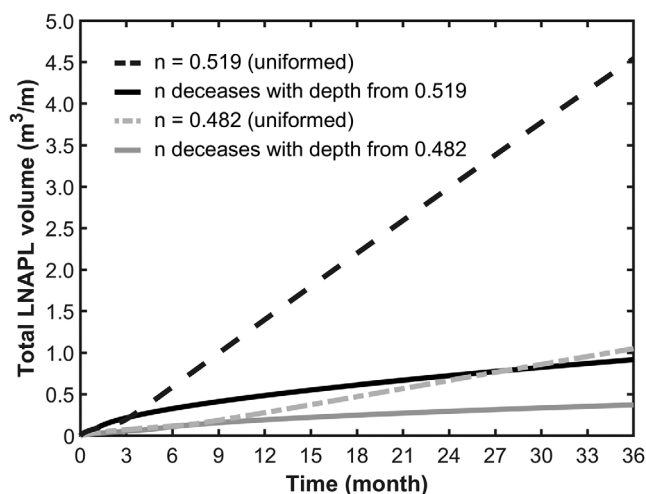


**FIGURE 13** Influence of porosity distribution through Series B2: total light non-aqueous phase liquid (LNAPL) volume

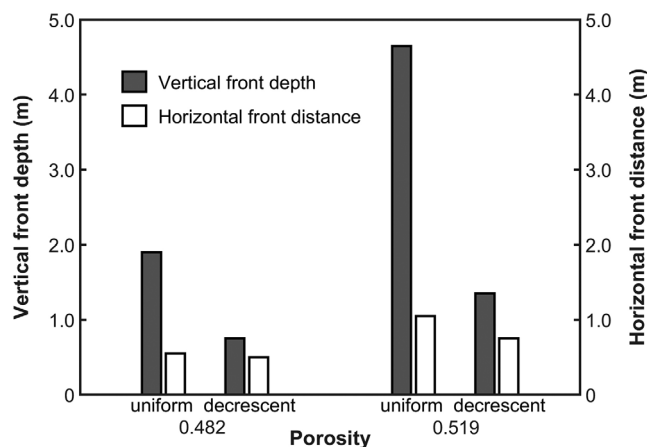


**FIGURE 14** Influence of porosity distribution through Series B2: vertical front depth and horizontal front distance (uniform: soil porosity is constant along the depth; descent: soil porosity decreases with increasing depth because of the compression under soil self-weight)

Figure 14. In the range of higher porosity, the total LNAPL volume is more sensitive to the change in soil porosity. In addition, the descent porosity resulted in a higher water retention capacity and a higher initial water saturation than the uniform condition, which caused a lower accumulation rate of LNAPL infiltration.

The porosity distribution also affects the shape of the contaminated zone in the ground, as illustrated by the ratio of the vertical front depth to the horizontal front depth in Figure 14. When the distribution is changed from uniform to descent conditions, the vertical front depth at 36 mo reduces to 30% for  $n = 0.519$  and 40% for  $n = 0.482$ . As expected, the horizontal front distance does not show obvious changes. In the field, the porosity generally decreases along with the depth. In most of the numerical simulations (Lari, Davis, et al., 2016; Lenhard & Parker, 1990; Lenhard et al., 2018; Pasha et al.,



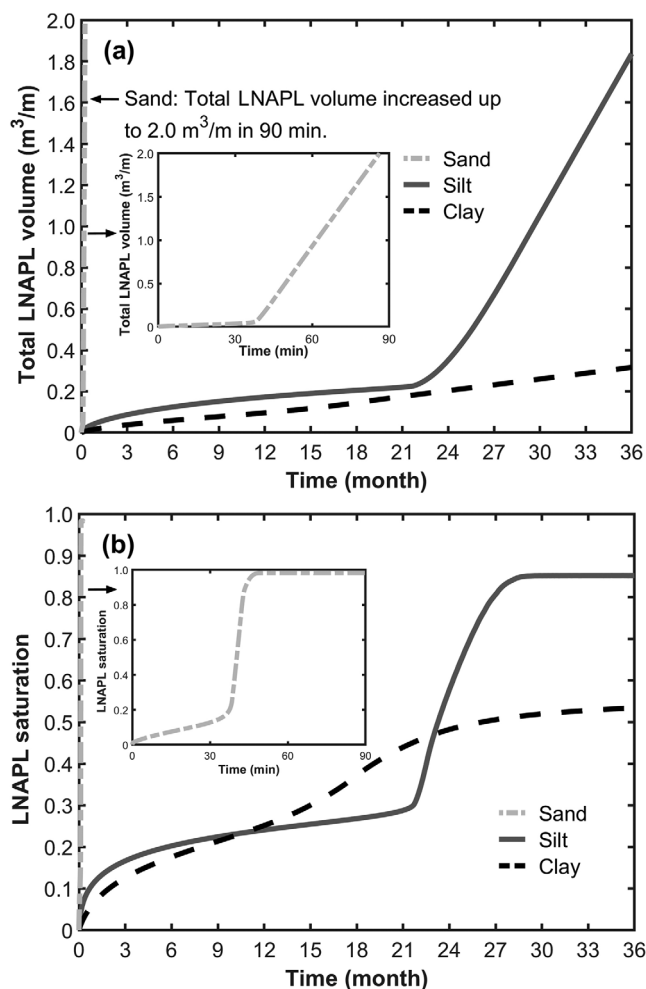


**FIGURE 15** Influence of soil type obtained through Series B3: (a) total light non-aqueous phase liquid (LNAPL) volume; (b) average LNAPL saturation in the sampling area at 36 mo

2014), however, the porosity is assumed to be uniform. This simplification would greatly overestimate the zone of contaminated ground, particularly in the vertical direction, if the behavior of shallow soils is used to calibrate soil parameters.

### 6.3 | Influence of soil type and layering on LNAPL flow

Figure 15a shows the total volume of LNAPL leaked into the ground. Three types of soil are considered in Series B3, including sand, silt, and clay. As expected, the largest accumulating rate was obtained in the sand. The LNAPL volume in the sand increases to  $2.0 \text{ m}^3 \text{ m}^{-1}$  in 90 min, whereas it takes 36 mo to reach  $1.8 \text{ m}^3 \text{ m}^{-1}$  in the silt. At 36 mo, the LNAPL volume in the clay is about  $0.32 \text{ m}^3 \text{ m}^{-1}$ , which is only about one-sixth of that in the silt. It can be concluded that, given the same leak source, coarse-grained soil (sand) could cause a much larger LNAPL volume than fine-grained soils (silt

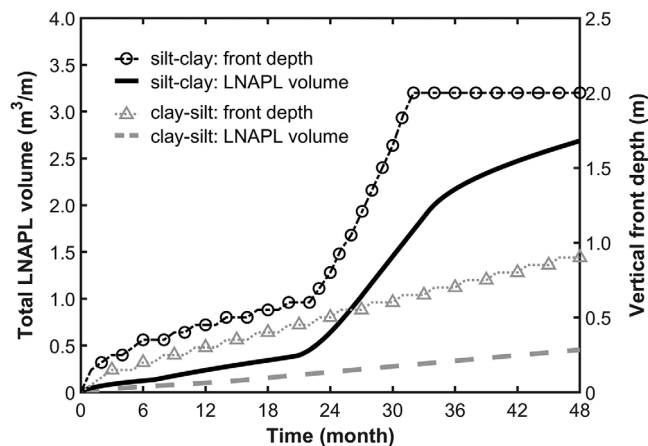


**FIGURE 16** Influence of layering obtained through Series B4: vertical front depth and total light non-aqueous phase liquid (LNAPL) volume

and clay). This is mainly attributed to the different intrinsic permeabilities of these soils, as explained by some previous researchers (Beckett & Huntley, 1998; Lari et al., 2018).

Silt and sand clearly show a bilinear relationship between the total LNAPL volume and time, similar to the results of clay in Figure 11. However, the nonlinearity in sand and silt is much more obvious than that in clay. This is because sand and silt have a lower retention capacity than clay. The initial water saturation prior to the LNAPL leakage is lower (initial water saturation at the ground surface: <1% for sand, 14.7% for silt, 45.8% for clay). Hence, the LNAPL saturation can show a larger increment and therefore alter the relative permeability of LNAPL more significantly. On the other hand, the infiltration rate of LNAPL in the silt is close to that in the clay before the turning point at about 21 mo. This can be explained by the retention behavior and relative permeability of water and LNAPL. The levels of LNAPL saturation in the clay and silt are very close (see Figure 15b); the LNAPL saturation is the average saturation in a 0.25-m-deep and 1.0-m-wide area under the leak source, which is highly related to the LNAPL accumulation rate and leak volume) before 21 mo. Water saturation in the clay is higher than that in the silt because clay has greater water retention. Following Equation 10, the higher water saturation in the clay leads to a larger relative permeability of LNAPL. This would compensate for the effects of a lower intrinsic permeability of clay. Thus, the clay and silt grounds show a similar response at the early stage. However, when the accumulated LNAPL volume in the ground is large enough, the relative permeability becomes closer to 1, and the intrinsic permeability plays a dominant role.

Figure 16 shows the influence of soil layering on the total LNAPL volume and vertical front depth. Two ground conditions are compared in Series B4: the silt-clay case (i.e., clay lies under silt) and the clay-silt case (silt lies under clay). For the silt-clay case, the increase rate of total LNAPL volume



and vertical front depth becomes much smaller after 34 mo due to the barrier effects of underlying lower-permeability clay. This is primarily because of the intrinsic permeability difference discussed in Series B3. On the other hand, due to retention behavior differences, there is greater LNAPL–water capillary pressure in the clay than in the silt. When the LNAPL front reaches the interface (2.0 m depth), the front can hardly infiltrate into the clay layer until the LNAPL pressure overcome the LNAPL–water capillary pressure in the clay layer. Similar barrier effects on LNAPL flow were reported by Soga et al. (2003) in both centrifuge experiments and numerical simulations. In the clay–silt case, the underlying higher-permeability silt does not show an obvious influence on the flow of LNAPL and leak volume. Under a consistently low infiltration rate in the clay layer, the LNAPL front depth reaches only 0.9 m after 48 mo. The LNAPL volume is  $0.46 \text{ m}^3 \text{ m}^{-1}$  in the clay–silt case, almost one-sixth of that in the silt–clay case. The results suggest that the barrier effects by lower-permeability clay can prevent a large leak rate. Hence, site selection or using replacement methods is crucial for the prevention of intense LNAPL contamination.

The computed results of LNAPL migration could be affected by numerical conditions, such as mathematic formulations, model parameters, boundary conditions, water content distribution, assumptions in governing equations, etc. The field conditions are much more complicated than the numerical model presented in this study, so the computed results above should be applied with caution by considering the potential influence of various factors. For instance, Figure 10 suggests an infiltration depth of 5 m in 3 yr. This infiltration rate seems high, with reference to the LNAPL infiltration rates in typical intact clay. Such a high infiltration rate may be attributed to two facts and may not be generalized: (a) the initial water saturation prior to LNAPL leakage is only 50%, and (b) it was reported by previous researchers that the intrinsic permeability is generally in the range of  $10^{-14}$ – $10^{-19} \text{ m}^2$  for clay and  $10^{-1}$ – $10^{-15} \text{ m}^2$  for silt (Bear, 1988). The selected clay has an intrinsic permeability of  $2 \times 10^{-15} \text{ m}^2$  in UP1 (Zhang et al., 2020), and this value is clearly very large among clays.

## 7 | SUMMARY AND CONCLUSIONS

A new theoretical model was developed to simulate LNAPL flow in the vadose zone. It considers porosity effects on soil hydraulic properties, including the water/LNAPL retention behavior and water/LNAPL permeability function, on the basis of experimental results. By using this model, a finite difference code was developed in MATLAB and verified using the results of a centrifuge test. Using the new code, comprehensive parametric studies were carried out to investigate the

flow of LNAPL upon its leakage at the ground surface. At the leakage source, the pressure of LNAPL was maintained constant. Based on the results of parametric studies, the following conclusions can be drawn.

The wetting front and leakage volume of LNAPL are greatly affected by soil porosity. For example, as the porosity of clay increases from 0.408 to 0.519, the depth of the wetting front increases from 0.25 to 4.65 m, and leakage volume accumulated over 36 mo increases from 0.09 to  $3.84 \text{ m}^3 \text{ m}^{-1}$ . These are mainly attributed to porosity effects on soil hydraulic properties: (a) the intrinsic permeability is larger at a higher porosity, and (b) the water saturation prior to the LNAPL leakage is lower at a higher porosity. The degree of saturation and relative permeability of LNAPL is therefore larger. Moreover, these results imply that heavy compaction can be applied to minimize the LNAPL contamination effectively.

The wetting front and leak volume of LNAPL increase nonlinearly with an increase in porosity, at an increasing rate. When the porosity is below a critical value (0.45 for the clay investigated), the variation of porosity does not show a significant effect. If the porosity exceeds the critical value, porosity effects become much more important. The observed nonlinearity is because of the highly nonlinear relationship between soil porosity and intrinsic permeability.

Compared with the case of descent porosity along with the depth, the leakage volume accumulated over 36 mo in the case of uniform porosity is about 3.5 and 2.5 times larger when the surface porosity is 0.519 and 0.482, respectively. A similar trend was observed for the depth of the wetting front and the area of the contaminated zone. This suggests that if a numerical model does not consider porosity effects and the behavior of shallow soils is used to calibrate model parameters, it greatly overestimates LNAPL contamination.

The relationship between the leakage volume of LNAPL and time is clearly bilinear (a smaller leakage rate at the first stage) in the sand and silt ground, whereas it is almost linear in the clay ground. This is likely because sand and silt have lower retention capacities and hence lower water saturation prior to the leakage of LNAPL. Thus, the saturation and relative permeability of LNAPL can vary in a much wider range, resulting in the different leakage rates at different stages. In addition, the existence of a bilinear relationship suggests that it is much more efficient to control LNAPL flow at the first stage.

In the ground consisting of distinct soil layers, the barrier effects of underlying lower-permeability clay are very significant. In the silt–clay case, the wetting front of LNAPL almost keeps constant after it reaches the soil interface, and the leakage rate of LNAPL becomes much smaller. In the clay–silt case, the overlying clay layer limits the LNAPL infiltration from the beginning.

## ACKNOWLEDGMENTS

This work was supported by the National Science Foundation of China through Research Grant 52022004. The authors thank the Research Grants Council (RGC) of the HKSAR (16204817), the Natural Science Foundation of Shaanxi Province (2020JQ-041), and the Technology Innovation Center for Land Engineering and Human Settlements, Shaanxi Land Engineering Construction Group Co., Ltd and Xi'an Jiaotong University (201912131-A1).

## AUTHOR CONTRIBUTIONS

Jia-ren Yu: Data curation; Formal analysis; Investigation; Methodology; Software; Validation; Visualization; Writing-original draft. Chao Zhou: Conceptualization; Funding acquisition; Methodology, Project administration; Supervision; Writing-review & editing. Qing Yi MU: Formal analysis; Validation; Writing-review & editing.

## CONFLICT OF INTEREST

The authors declare no conflict of interest.

## ORCID

Jia-ren Yu  <https://orcid.org/0000-0003-4419-484X>

Chao Zhou  <https://orcid.org/0000-0002-9443-6707>

Qing Yi Mu  <https://orcid.org/0000-0002-9235-4978>

## REFERENCES

- Aral, M. M., & Liao, B. (2000). LNAPL thickness interpretation based on bail-down tests. *Groundwater*, 38(5), 696–701. <https://doi.org/10.1111/j.1745-6584.2000.tb02705.x>
- Aziz, K. (1979). *Petroleum reservoir simulation*. Applied Science Publishers.
- Bear, J. (1988). *Dynamics of fluids in porous media*. Courier Corporation.
- Beckett, G., & Huntley, D. (1998). Soil properties and design factors influencing free-phase hydrocarbon cleanup. *Environmental Science & Technology*, 32(2), 287–293.
- Brooks, R., & Corey, A. (1964). *Hydraulic properties of porous media*. Civil Engineering Department, Colorado State University.
- Busby, R. D., Lenhard, R. J., & Rolston, D. E. (1995). An investigation of saturation-capillary pressure relations in two-and three-fluid systems for several NAPLS in Different porous media. *Groundwater*, 33(4), 570–578. <https://doi.org/10.1111/j.1745-6584.1995.tb00312.x>
- Carman, P. C. (1939). Permeability of saturated sands, soils and clays. *The Journal of Agricultural Science*, 29(2), 262–273. <https://doi.org/10.1017/S0021859600051789>
- Corey, A. T. (1994). *Mechanics of immiscible fluids in porous media*. Water Resources Publication.
- Cui, Y. J., Delage, P., & Alzoghbi, P. (2003). Retention and transport of a hydrocarbon in a silt. *Géotechnique*, 53(1), 83–91. <https://doi.org/10.1680/geot.2003.53.1.83>
- Delshad, M., Asakawa, K., Pope, G. A., & Sepehrnoori, K. (2002). *Simulations of chemical and microbial enhanced oil recovery methods* [Paper presentation]. SPE/DOE Improved Oil Recovery Symposium, Tulsa, OK.
- Falta, R. W., Pruess, K., Finsterle, S., & Battistelli, A. (1995). *T2VOC user's guide*. Ernest Orlando Lawrence Berkeley National Laboratory.
- Gallage, C. P. K., & Uchimura, T. (2010). Effects of dry density and grain size distribution on soil-water characteristic curves of sandy soils. *Soils and Foundations*, 50(1), 161–172. <https://doi.org/10.3208/sandf.50.161>
- Gallipoli, D., Wheeler, S. J., & Karstunen, M. (2003). Modelling the variation of degree of saturation in a deformable unsaturated soil. *Géotechnique*, 53(1), 105–112. <https://doi.org/10.1680/geot.2003.53.1.105>
- Guarnaccia, J., Pinder, G., & Fishman, M. (1997). *NAPL: Simulator documentation*. National Risk Management Research Laboratory, USEPA.
- Hammond, G. E., Lichtner, P. C., & Mills, R. T. (2014). Evaluating the performance of parallel subsurface simulators: An illustrative example with PFLOTTRAN. *Water Resources Research*, 50(1), 208–228. <https://doi.org/10.1002/2012WR013483>
- Helmig, R., & Huber, R. (1998). Comparison of Galerkin-type discretization techniques for two-phase flow in heterogeneous porous media. *Advances in Water Resources*, 21(8), 697–711. [https://doi.org/10.1016/S0309-1708\(97\)00023-7](https://doi.org/10.1016/S0309-1708(97)00023-7)
- Hu, R., Chen, Y.-F., Liu, H.-H., & Zhou, C.-B. (2013). A water retention curve and unsaturated hydraulic conductivity model for deformable soils: Consideration of the change in pore-size distribution. *Géotechnique*, 63(16), 1389–1405. <https://doi.org/10.1680/geot.12.P.182>
- Jackson, R. E., Dwarakanath, V., Ewing, J. E., & Avis, J. (2006). Migration of viscous non-aqueous phase liquids (NAPLs) in alluvium, Fraser River lowlands, British Columbia. *Canadian Geotechnical Journal*, 43(7), 694–703. <https://doi.org/10.1139/t06-034>
- Jarvis, N. J., & Messing, I. (1995). Near-saturated hydraulic conductivity in soils of contrasting texture measured by tension infiltrometers. *Soil Science Society of America Journal*, 59(1), 27–34. <https://doi.org/10.2136/sssaj1995.03615995005900010004x>
- Jeong, J., & Charbeneau, R. J. (2014). An analytical model for predicting LNAPL distribution and recovery from multi-layered soils. *Journal of Contaminant Hydrology*, 156, 52–61. <https://doi.org/10.1016/j.jconhyd.2013.09.008>
- Johnston, C. D., & Trefry, M. G. (2009). Characteristics of light non-aqueous phase liquid recovery in the presence of fine-scale soil layering. *Water Resources Research*, 45(5), <https://doi.org/10.1029/2008WR007218>
- Koponen, A., Kataja, M., & Timonen, J. (1997). Permeability and effective porosity of porous media. *Physical Review E*, 56(3), 3319. <https://doi.org/10.1103/PhysRevE.56.3319>
- Lekmine, G., Sookhak Lari, K., Johnston, C. D., Bastow, T. P., Rayner, J. L., & Davis, G. B. (2017). Evaluating the reliability of equilibrium dissolution assumption from residual gasoline in contact with water saturated sands. *Journal of Contaminant Hydrology*, 196, 30–42. <https://doi.org/10.1016/j.jconhyd.2016.12.003>
- Lenhard, R. J., & Parker, J. C. (1990). Estimation of free hydrocarbon volume from fluid levels in monitoring wells. *Groundwater*, 28(1), 57–67. <https://doi.org/10.1111/j.1745-6584.1990.tb02229.x>
- Lenhard, R. J., Rayner, J. L., & Davis, G. B. (2017). A practical tool for estimating subsurface LNAPL distributions and transmissivity using current and historical fluid levels in groundwater wells: Effects of entrapped and residual LNAPL. *Journal of Contaminant Hydrology*, 205, 1–11. <https://doi.org/10.1016/j.jconhyd.2017.06.002>

- Lenhard, R. J., Sookhak, K., Rayner, J. L., & Davis, G. B. (2018). Evaluating an analytical model to predict subsurface LNAPL distributions and transmissivity from current and historic fluid levels in groundwater wells: Comparing results to numerical simulations. *Groundwater Monitoring & Remediation*, 38(1), 75–84.
- Leong, E. C., & Rahardjo, H. (1997). Permeability functions for unsaturated soils. *Journal of Geotechnical and Geoenvironmental Engineering*, 123(12), 1118–1126. [https://doi.org/10.1061/\(ASCE\)1090-0241\(1997\)123:12\(1118\)](https://doi.org/10.1061/(ASCE)1090-0241(1997)123:12(1118))
- Leverett, M. C. (1941). Capillary behavior in porous solids. *Transactions of the AIME*, 142(01), 152–169. <https://doi.org/10.2118/941152-G>
- Leverett, M. C., & Lewis, W. B. (1941). Steady flow of gas-oil-water mixtures through unconsolidated sands. *Transactions of the AIME*, 142(01), 107–116. <https://doi.org/10.2118/941107-G>
- McWhorter, D. B., & Sunada, D. K. (1990). Exact integral solutions for two-phase flow. *Water Resources Research*, 26(3), 399–413. <https://doi.org/10.1029/WR026i003p00399>
- Mualem, Y. (1976). A new model for predicting the hydraulic conductivity of unsaturated porous media. *Water Resources Research*, 12(3), 513–522. <https://doi.org/10.1029/WR012i003p00513>
- Ng, C. W. W., & Pang, Y. W. (2000). Experimental investigations of the soil-water characteristics of a volcanic soil. *Canadian Geotechnical Journal*, 37(6), 1252–1264. <https://doi.org/10.1139/t00-056>
- Ng, C. W. W., Zhou, C., & Chiu, C. F. (2020). Constitutive modelling of state-dependent behaviour of unsaturated soils: An overview. *Acta Geotechnica*, 15(10), 2705–2725. <https://doi.org/10.1007/s11440-020-01014-7>
- Oostrom, M., & Lenhard, R. J. (1998). Comparison of relative permeability-saturation-pressure parametric models for infiltration and redistribution of a light nonaqueous-phase liquid in sandy porous media. *Advances in Water Resources*, 21(2), 145–157. [https://doi.org/10.1016/S0309-1708\(96\)00038-3](https://doi.org/10.1016/S0309-1708(96)00038-3)
- Parker, J. C., Lenhard, R. J., & Kuppusamy, T. (1987). A parametric model for constitutive properties governing multiphase flow in porous media. *Water Resources Research*, 23(4), 618–624. <https://doi.org/10.1029/WR023i004p00618>
- Pasha, A. Y., Hu, L., & Meegoda, J. N. (2014). Numerical simulations of a light nonaqueous phase liquid (LNAPL) movement in variably saturated soils with capillary hysteresis. *Canadian Geotechnical Journal*, 51(9), 1046–1062. <https://doi.org/10.1139/cgj-2012-0165>
- Pruess, K. (2004). The TOUGH codes—A family of simulation tools for multiphase flow and transport processes in permeable media. *Vadose Zone Journal*, 3(3), 738–746. <https://doi.org/10.2136/vzj2004.0738>
- Pruess, K., & Battistelli, A. (2002). *TMVOC, a numerical simulator for three-phase non-isothermal flows of multicomponent hydrocarbon mixtures in saturated-unsaturated heterogeneous media*. Ernest Orlando Lawrence Berkeley National Laboratory.
- Rivett, M. O., Tomlinson, D. W., Thornton, S. F., Thomas, A. O., Leharne, S. A., & Wealthall, G. P. (2014). *An illustrated handbook of LNAPL transport and fate in the subsurface*. Environment Agency.
- Salager, S., Nuth, M., Ferrari, A., & Laloui, L. (2013). Investigation into water retention behaviour of deformable soils. *Canadian Geotechnical Journal*, 50(2), 200–208. <https://doi.org/10.1139/cgj-2011-0409>
- Sale, T., Hopkins, H., & Kirkman, A. (2018). Managing risk at LNAPL sites—Frequently asked questions. In T. Sale, H. Hopkins, & A. Kirkman (Eds.), *API Soil and Research Bulletin Number 18*. API.
- Schmid, K. S., Geiger, S., & Sorbie, K. S. (2011). Semianalytical solutions for cocurrent and countercurrent imbibition and dispersion of solutes in immiscible two-phase flow. *Water Resources Research*, 47(2), <https://doi.org/10.1029/2010WR009686>
- Sharmin, N., & Gabr, M. A. (2012). Optimized prefabricated vertical wells for light nonaqueous phase liquid recovery. *Canadian Geotechnical Journal*, 49(12), 1434–1443. <https://doi.org/10.1139/t2012-097>
- Soga, K., Kawabata, J., Kechavarzi, C., Coumoulos, H., & Waduge, W. A. P. (2003). Centrifuge modeling of nonaqueous phase liquid movement and entrapment in unsaturated layered soils. *Journal of Geotechnical and Geoenvironmental Engineering*, 129(2), 173–182. [https://doi.org/10.1061/\(ASCE\)1090-0241\(2003\)129:2\(173\)](https://doi.org/10.1061/(ASCE)1090-0241(2003)129:2(173))
- Sookhak, K., Davis, G. B., & Johnston, C. D. (2016). Incorporating hysteresis in a multi-phase multi-component NAPL modelling framework; a multi-component LNAPL gasoline example. *Advances in Water Resources*, 96, 190–201. <https://doi.org/10.1016/j.advwatres.2016.07.012>
- Sookhak, K., Davis, G. B., Rayner, J. L., Bastow, T. P., & Puzon, G. J. (2019). Natural source zone depletion of LNAPL: A critical review supporting modelling approaches. *Water Research*, 157, 630–646. <https://doi.org/10.1016/j.watres.2019.04.001>
- Sookhak, K., Johnston, C. D., & Davis, G. B. (2016). Gasoline multiphase and multicomponent partitioning in the vadose zone: Dynamics and risk longevity. *Vadose Zone Journal*, 15(3), <https://doi.org/10.2136/vzj2015.07.0100>
- Sookhak, K., Rayner, J. L., & Davis, G. B. (2018). Towards characterizing LNAPL remediation endpoints. *Journal of Environmental Management*, 224, 97–105. <https://doi.org/10.1016/j.jenvman.2018.07.041>
- Sookhak, K., Rayner, J. L., & Davis, G. B. (2019). Toward optimizing LNAPL remediation. *Water Resources Research*, 55(2), 923–936. <https://doi.org/10.1029/2018WR023380>
- Stoltz, G., Gourc, J.-P., & Oxarango, L. (2010). Liquid and gas permeabilities of unsaturated municipal solid waste under compression. *Journal of Contaminant Hydrology*, 118(1–2), 27–42. <https://doi.org/10.1016/j.jconhyd.2010.07.008>
- Tarantino, A. (2009). A water retention model for deformable soils. *Géotechnique*, 59(9), 751–762. <https://doi.org/10.1680/geot.7.00118>
- Van Genuchten, M. T. (1980). A closed-form equation for predicting the hydraulic conductivity of unsaturated soils. *Soil Science Society of America Journal*, 44(5), 892–898. <https://doi.org/10.2136/sssaj1980.03615995004400050002x>
- White, M. D., & Oostrom, M. (2003). *STOMP subsurface transport over multiple phases version 3.0 User's guide*. U.S. Department of Energy, Office of Scientific and Technical Information.
- Yang, Z., Zandin, H., Niemi, A., & Fagerlund, F. (2013). The role of geological heterogeneity and variability in water infiltration on non-aqueous phase liquid migration. *Environmental Earth Sciences*, 68(7), 2085–2097. <https://doi.org/10.1007/s12665-012-1894-6>
- Yoon, H., Werth, C. J., Valocchi, A. J., & Oostrom, M. (2008). Impact of nonaqueous phase liquid (NAPL) source zone architecture on mass removal mechanisms in strongly layered heterogeneous porous media during soil vapor extraction. *Journal of Contaminant Hydrology*, 100(1–2), 58–71. <https://doi.org/10.1016/j.jconhyd.2008.05.006>
- Zhang, D., Wang, J., & Chen, C. (2020). Gas and liquid permeability in the variably saturated compacted loess used as an earthen final cover material in landfills. *Waste Management*, 105, 49–60. <https://doi.org/10.1016/j.wasman.2020.01.030>

- Zhou, A.-N., Sheng, D., & Carter, J. P. (2012). Modelling the effect of initial density on soil-water characteristic curves. *Géotechnique*, 62(8), 669–680. <https://doi.org/10.1680/geot.10.P.120>
- Zhou, C., & Chen, R. (2021). Modelling the water retention behaviour of anisotropic soils. *Journal of Hydrology*, 599, 126361. <https://doi.org/10.1016/j.jhydrol.2021.126361>
- Zhou, C., & Ng, C. W. W. (2014). A new and simple stress-dependent water retention model for unsaturated soil. *Computers and Geotechnics*, 62, 216–222. <https://doi.org/10.1016/j.compgeo.2014.07.012>
- Zhou, C., So, P. S., & Chen, X. W. (2020). A water retention model considering biopolymer-soil interactions. *Journal of Hydrology*, 586, 124874. <https://doi.org/10.1016/j.jhydrol.2020.124874>
- Zhou, C., Tai, P., & Yin, J.-H. (2020). A bounding surface model for saturated and unsaturated soil-structure interfaces. *International Journal for Numerical and Analytical Methods in Geomechanics*, 44(18), 2412–2429. <https://doi.org/10.1002/nag.3123>

**How to cite this article:** Yu, J., Zhou, C., & Mu, Q. (2022). Numerical investigation on light non-aqueous phase liquid flow in the vadose zone considering porosity effects on soil hydraulic properties. *Vadose Zone Journal*, 21, e20211. <https://doi.org/10.1002/vzj2.20211>

## APPENDIX A: Parameterization for the solid–water–LNAPL–air system

Volumetric fractions of these four phases can be described using the following variables:

$$n = \frac{V_A + V_N + V_W}{V_A + V_N + V_W + V_S} \quad (\text{A1})$$

$$S_W = \frac{V_W}{V_A + V_W + V_N} \quad (\text{A2})$$

$$S_N = \frac{V_N}{V_A + V_W + V_N} \quad (\text{A3})$$

$$S_t = S_W + S_N \quad (\text{A4})$$

where  $n$  is the porosity;  $S_W$  and  $S_N$  are the water and LNAPL saturation, respectively; and their sum  $S_t$  is the total liquid saturation, so the air saturation is thus equal to  $(1 - S_t)$ ; and  $V$  with the subscripts are the volumes of the above four phases. In addition, the following two variables are defined and used:

$$\bar{S}_W = \frac{S_W - S_m}{1 - S_m} \quad (\text{A5})$$

$$\bar{S}_t = \frac{S_t - S_m}{1 - S_m} \quad (\text{A6})$$

where  $\bar{S}_W$  and  $\bar{S}_t$  are the effective water saturation and effective total liquid saturation, respectively;  $S_m$  is the residual degree of saturation, which is also referred to the apparent minimum or “irreducible” wetting fluid saturation in the literature (e.g., Parker et al., 1987).

When multiple types of fluid are present in the soil, they interact with each other, resulting in curved interfaces. The pressure difference across an interface is defined as capillary pressure. For instance, if water, LNAPL, and air are all present in the soil, water pressure is the smallest because of its highest wettability, whereas air pressure is the largest due to its lowest wettability (Aziz, 1979). The difference between air pressure ( $P_A$ ) and water pressure ( $P_W$ ) is defined as the air–water capillary pressure ( $P_{cAW}$ ):

$$P_{cAW} = P_A - P_W \quad (\text{A7})$$

Similarly, the air–LNAPL capillary pressure ( $P_{cAN}$ ) and LNAPL–water capillary pressure ( $P_{cNW}$ ) are defined as follows:

$$P_{cAN} = P_A - P_N \quad (\text{A8})$$

$$P_{cNW} = P_N - P_W \quad (\text{A9})$$

where  $P_N$  is the LNAPL pressure.

## APPENDIX B: Mass balance and Darcy’s law

The mass balance equation for the water phase is as follows (Aziz, 1979):

$$\rho_W \left( \nabla \cdot \mathbf{v}_W n \frac{\partial S_W}{\partial t} \right) = Q_W \quad (\text{B1})$$

where  $\rho_W$  is the density of water ( $\text{kg m}^{-3}$ ),  $\mathbf{v}_W$  is the Darcy flux (or Darcy velocity) vector of water ( $\text{m s}^{-1}$ ),  $t$  is the time (s), and  $Q_W$  is the source-sink term for the water ( $\text{kg m}^{-3} \text{s}^{-1}$ ). The Darcy flux of water flow in Equation B1 is described using Darcy’s law:

$$\mathbf{v}_W = -\frac{k_W}{\mu_W} \cdot (\nabla P_W - \rho_W g \nabla z) \quad (\text{B2})$$

where  $K_W$  is the effective permeability of water ( $\text{m}^2$ );  $\mu_W$  is the dynamic viscosity of water ( $\text{N s}^{-1} \text{m}^{-2}$ );  $\nabla P_W$  is the gradient of water pressure;  $g$  is the gravitational acceleration, which is equal to  $9.8 \text{ m s}^{-2}$ ; and  $z$  is the elevation (m).

Through experimental investigations, Darcy’s law has been found applicable for the flow of LNAPL in porous media (Leverett & Lewis, 1941). Hence, the following two equations



are derived for LNAPL flow based on Darcy's law and mass conservation:

$$\rho_N \left( \nabla \cdot \mathbf{v}_N + n \frac{\partial S_N}{\partial t} \right) = Q_N \quad (\text{B3})$$

$$\mathbf{v}_N = -\frac{k_N}{\mu_N} \cdot (\nabla P_N - \rho_N - g \nabla z) \quad (\text{B4})$$

where  $\rho_N$  is the density of LNAPL ( $\text{kg m}^{-3}$ ),  $\mathbf{v}_N$  is the Darcy flux (or Darcy velocity) vector of LNAPL ( $\text{m s}^{-1}$ ),  $Q_N$  ( $\text{kg m}^{-3} \text{ s}^{-1}$ ) is the source-sink term for LNAPL,  $k_N$  is the effective permeability of LNAPL ( $\text{m}^2$ ), and  $\mu_N$  is the dynamic viscosity of LNAPL ( $\text{N s}^{-1} \text{ m}^{-2}$ ).

### APPENDIX C: Water retention model for LNAPL-contaminated soil

For unsaturated soils (i.e., an air–water–solid three-phase system), the model of van Genuchten (1980) is widely used for the S–P relation:

$$P_{\text{cAW}} = \left[ (\bar{S}_W)^{-1/m} - 1 \right]^{1-m} \alpha^{-1} \quad (\text{C1})$$

where  $m$  and  $\alpha$  are model parameters. Parameter  $m$  considers the influence of pore size distribution. Parameter  $\alpha$  is inversely proportional to the displacement pressure. Some researchers (e.g., Parker et al., 1987) have demonstrated that this equation can be applied to describe the water retention behavior of LNAPL-contaminated unsaturated soils (a solid–water–LNAPL–air four-phase system) with some minor modifications: (a) the water saturation depends on the LNAPL–water capillary pressure, and (b) the entry capillary pressure of a given pore is proportional to the interfacial tension of fluids, according to the classic Young–Laplace equation. Thus, a fluid type–dependent scaling factor  $\beta_{\text{NW}}$  is introduced to the account for the influence of interfacial tension (Corey, 1994):

$$\beta_{\text{NW}} = T_{\text{AW}}/T_{\text{NW}} \quad (\text{C2})$$

By applying the above two modifications, it is derived from Equation C2 that

$$P_{\text{cNW}} = \left[ (\bar{S}_W)^{-1/m} - 1 \right]^{1-m} \alpha^{-1} \beta_{\text{NW}}^{-1} \quad (\text{C3})$$